Supporting Information Appendix

Van Kooten et al.

Materials and Methods

Metal-rich carbonaceous chondrites and their components

CR, CH and CB carbonaceous chondrites distinguish themselves from other carbonaceous chondrites by their high metal content, elevated $^{15}N/^{14}N$ ratio and distinct bulk oxygen isotope compositions [1,2]. In spite of bulk chemical and isotopic similarities between these chondrite groups, there are significant differences in their mineralogy and petrology, briefly described below.

CR chondrites consist of three major components chondrules, Fe,Ni-metal, and interstitial fine-grained matrix. Refractory inclusions [Ca,Al-rich inclusions (CAIs) and amoeboid olivine aggregates (AOAs)] are very rare. Most refractory inclusions have ^{16}O-rich compositions ($\Delta^{17}O \sim -25‰$) and high initial $^{26}Al/^{27}Al$ ratios ($(^{26}Al/^{27}Al)_0 \leq (4\text{-}5)\times10^{-5}$)[3]. Most chondrules have porphyritic textures, magnesium-rich compositions, and low $(^{26}Al/^{27}Al)_0$ of $<6\times10^{-6}$ [4]. CR chondrites experienced aqueous alteration to various degrees at relatively low temperature (<100°C), but avoided thermal metamorphism [5,6].

CB chondrites consist mainly of Fe,Ni-metal (up to 70 vol%) and chondrules. CAIs are exceptionally rare and the fine-grained interstitial matrix is absent. Heavily-hydrated lithic clasts are found in some CB chondrites [7]. Most CAIs have igneous textures, ^{16}O-depleted compositions and lack resolvable excess of ^{26}Mg* [8]. The CB chondrules have magnesium-rich compositions and non-porphyritic textures (skeletal and cryptocrystalline). It is generally accepted that chondrules and metal grains in CB chondrites formed in an impact generated plume ∼5 Myr after the birth of the solar system [9]. CAIs could have been melted in this plume [8].

Isheyevo is a CH/CB$_b$-chondrite that consists of two lithologies, namely a dominant metal-rich lithology similar to CB chondrites (50-90vol% Fe,Ni metal) and a silicate-rich lithology similar to CH chondrites (7-50 vol% Fe,Ni metal). Both lithologies contain metal, chondrules, refractory inclusions and hydrated lithic clasts, although they show variations in modal abundances, chondrule size and proportions of porphyritic versus non-porphyritic chondrules [10]. The hydrated lithic clasts in Isheyevo are thought to represent previously unsampled parent material(s) and were incorporated into the Isheyevo host after/while it formed from the impact-vapor/melt plume that also produced CH and CB chondrites [9]. These lithic clasts can be divided into three main groups [11]. Isheyevo, like other metal-rich carbonaceous chondrites, is characterized by high enrichments of ^{15}N in the bulk rock ($\delta^{15}N>1000‰$ [10]). These enrichments in ^{15}N are thought to be related to the lithic clasts, which are characterized by the highest ^{15}N enrichments measured to date [12,13].

We have selected nine lithic clasts to constrain the timing of aqueous alteration on their parent body by ^{53}Mn-^{53}Cr dating (n=4) of carbonates as well as probe the Mg- and Cr-isotope composition (n=5) of their precursor material. All nine clasts are classified as group I [11] by their mineralogy/petrology and chemistry, which was determined using compositional images and chemical analyses derived by UH electron microprobe (EMPA, Hawaii). High resolution back-scattered electron (BSE) images of the lithic clasts were taken (Figs. S1 and S2), after which the carbonate crystals used for ^{53}Mn-^{53}Cr dating (n=6) were mapped with a 1-2 µm/pixel resolution in Mg, Ca, Al, S and Ni Kα X-rays (Fig. S2). The microprobe operated at 15 KeV accelerating voltage, with a 5nA beam current and 3 µm beam size. Additionally, we determined the chemical compositions of phyllosilicate matrices in 9 clasts and carbonate grains in (Tables S1 and S2), using a focused beam (5nA, 5µm, Ca, Mg, Fe, Mn, Si Kα X-rays). Group I lithic clasts consist of hydrated matrix material, which contains phyllosilicates (mainly serpentine solid solution) finely interwoven with organic matter that supposedly carries the ^{15}N-rich functional group [13]. Grains of platy sulfide, framboidal magnetite and carbonates dominate as products of aqueous alteration (Fig. S2). Carbonates are mainly calcian dolomites ($CaCO_3$ = 50-63 mol%), with Mg being replaced by Mn (1-8 wt%) and Fe (2-7 wt%) to varying degrees (Table S2). The compositions of fine-grained and large phyllosilicates in lithic clasts show significant variations in Fe/Mg ratios (Table S1). Moreover, the matrix compositions of lithic clasts overlap with CI, CM and CR chondrites (Fig. S3 and Table S1). The presence of complex carbonates in lithic clasts (e.g. dolomites and breunnerites) suggests a link to CI and CM chondrites. CR chondrites contain mostly calcitic carbonates, indicating different physicochemical conditions during alteration of the CR parent body.

Nine chondrules from Isheyevo were selected for Mg- and Cr-isotope analyses (Table 1 and Fig. S4). They can be divided in ferroan/magnesian porphyritic (n=2) and skeletal/barred chondrules (n=7), which are typically characterized by distinct oxygen isotope compositions [14]. The selected chondrules are derived from silicate-rich and metal-rich lithologies in Isheyevo. Moreover, three porphyritic and skeletal chondrules from CR chondrites (NWA 6043, NWA 801, LAP 02342) were sampled. Elemental maps were made by secondary electron microscopy (SEM; GEUS, Copenhagen) (Fig. S4). Porphyritic chondrules from Isheyevo are Mg-rich and contain forsterite phenocrysts in a Ca and Al-rich feldspathic mesostasis. Two out of nine chondrules have a Mg-rich igneous rim. Five out of nine chondrules have a skeletal texture, while one chondrule is barred. Three CR chondrules have a porphyritic texture with forsterite phenocrysts in a Ca and Al-rich mesostasis, with finegrained Ca-rich rims whereas one CR chondrule has a skeletal texture (Fig. S4).

Three bulk CR chondrites (NWA 6043, EET 92161, NWA 7837) were selected for Mg- and Cr-isotope analyses. In addition, we measured Mg- and Cr-isotope compositions of Ivuna (CI) and Jbilet Winselwan (CM) chondrites.

^{53}Mn-^{53}Cr systematics of hydrated lithic clasts in the Isheyevo chondrite

Six carbonates from four lithic clasts were selected for isotope measurements on the UH Cameca ims-1280 ion microprobe (Hawaii), based on the absence of silicon contamination from matrix or inclusions and the presence of smooth surfaces. We searched for variability in Mn content (2-10 wt%) to ensure a wide range of Mn/Cr ratios. Ion microprobe pits were confirmed on the EMP (Hawaii) after isotope measurements. A 100pA $^{16}O^-$ primary beam was focused to ∼10µm and was set to measure three chromium isotopes (^{50}Cr, ^{52}Cr and ^{53}Cr) in multi-collection mode on electron multipliers for 45s. Subsequently, ^{55}Mn was collected for 2s after a peak jump. Each measurement consisted of 125 cycles (45+2s). Prior to each measurement, the sample surface was pre-sputtered for 300s with a 100pA beam in a 15×15 µm raster. Mass resolving power was typically ∼5900 for ^{53}Cr and ∼4100 for ^{52}Cr. Typical count rates for ^{52}Cr were >1000 cps for standards and >100cps for samples. A synthesized calcite doped with Mn and Cr [15] was used as a standard in between sample measurements. The true ^{55}Mn/^{52}Cr ratio was determined on the EMP, by measuring and averaging spots surrounding the pits formed by ion probe measurements, or by measuring the true ratio beforehand. In spite of the heterogeneity of the calcite crystal (Mn/Cr = 0.2-1.8), this provides the most accurate means of measuring the relative sensitivity factor of Mn and Cr (RSF=(^{55}Mn/^{52}Cr$_{SIMS}$)/(^{55}Mn/^{52}Cr$_{EMP}$)) to correct the ^{55}Mn/^{52}Cr ratios. The atomic ratio was corrected for the presence of ^{53}Cr during Cr analyses on the EMP. The synthesized calcite was measured at 20 kV, with a 5 nA beam current and 10 µm beam size, using Ca, Mg, Si, Mn and Cr Kα X-rays. Garnet Verma, chromite USNM 117075, calcite, dolomite and rhodochrosite were used as standards.

After ion probe analyses, the ^{53}Cr/^{52}Cr and ^{55}Mn/^{52}Cr ratios are reduced using total counts ratios of 125 cycles to prevent a positive artificial bias due to the low count rate of Cr [16]. The ^{55}Mn/^{52}Cr ratio was corrected using the averaged RSF of all standard runs acquired during individual analytical sessions. The error on the ^{55}Mn/^{52}Cr ratio is propagated from the counting statistics error and the error on the RSF: $\sigma^{55}\mathrm{Mn}/^{52}\mathrm{Cr}_{corr} = [(\sigma^{55}\mathrm{Mn}/^{52}\mathrm{Cr}_{meas})^2 + (\sigma\mathrm{RSF})^2]^{0.5}$. The ^{53}Cr/^{52}Cr ratio was corrected for instrumental mass fractionation (IMF) using the synthesized calcite standard and then converted to delta notation using ^{53}Cr/^{52}Cr = 0.1134 as standard value. The error on ^{53}Cr/^{52}Cr is derived similarly to the ^{55}Mn/^{52}Cr error, from the counting statistics and error on the calcite standard ^{53}Cr/^{52}Cr ratio. From the propagated errors on the corrected ^{55}Mn/^{52}Cr and ^{53}Cr/^{52}Cr ratios, we calculate the slope from the datapoints using Isoplot 3.75 (Table S3, Fig. S5).

Ten spot analyzes of dolomite grains from four individual clasts yield a correlation in Mn/Cr and δ^{53}Cr space defining a statistically significant isochron (MSWD=0.87) corresponding to an initial ^{53}Mn/^{55}Mn ratio of (2.30±0.31)×10^{-6} and an intercept $\delta^{53}\mathrm{Cr}_i$ of 12.5±3.4‰. We find no significant relationship between δ^{53}Cr and 1/Cr (MWSD=11.05), which would be indicative of mixing between ^{53}Cr-rich and ^{53}Cr-poor reservoirs (Fig. S6) and, thus, we interpret the Mn/Cr-δ^{53}Cr correlation as a meaningful isochron dating the timing of aqueous alteration on the parent body of hydrated lithic clasts. The initial ^{53}Mn/^{55}Mn ratio of (2.30±0.31)×10^{-6} is systematically lower than that defined by CM and CI chondrites (Fig. S7), indicating that the timing of aqueous alteration on the hydrated clast parent body occurred $1.54^{+0.92}_{-1.11}$ Myr after that of CI and CM chondrites. As the clasts are thought to have experienced aqueous alteration on their parent prior to their incorporation in Isheyevo [10], our result supports the late accretion of the Isheyevo parent body relative to the parent bodies of CI and CM chondrites.

Magnesium and chromium isotope measurements

Five hydrated lithic clasts and nine chondrules from Isheyevo as well as three chondrules from CR chondrites (LAP 02342, NWA 801, NWA 6043) were sampled using a computer-assisted micro-drilling device. In addition, fresh fragments were extracted from the interior parts of the NWA7837 (∼250 mg), EET92161 (∼280 mg) and NWA 6043 (∼3 g) CR chondrites as well as the Jbilet Winselwan CM chondrite (two aliquots of ∼100 mg and ∼200 mg) and Ivuna CI chondrite (∼200 mg) and crushed to a fine powder with an agate pestle and mortar. All samples were digested with mixtures of HF-HNO_3 acids for 2 days using Parr bombs at 210°C, after which they were redissolved in aqua regia overnight. Magnesium and chromium were purified from sample matrices by ion exchange chromatography based on protocols developed in [17] and [18] and adapted for the typically smaller sample sizes processed in this study. In detail, Mg was separated using a six steps purification scheme that combines cation, anion, TODGA and Ni-spec resins [17]. The Cr-rich separate was retrieved from the second step of the Mg chemical purification [18] and further processed through a two- step scheme using TODGA resin [18]. An additional step using cation resin (AG50X8 200-400 mesh, 100µl resin volume) was added to the Cr separation method to remove sodium, organics (0.5M HNO_3) and potential remaining high field strength elements (1M HF). Afterwards, the Cr separates were dissolved in concentrated aqua regia for 1 week and concentrated HNO_3 for 3 days at 130°C to remove any remaining organics. Chemistry yields for Mg and Cr are >99% and >95% respectively. Total Mg and Cr procedural blanks were less than 5 ng and 0.5 ng, respectively, and, thus, negligible for all samples analyzed in this study.

The isotopic composition of the purified Mg was determined using the Neptune MC-ICPMS *Plus* at the Centre for Star and Planet Formation, Natural History Museum of Denmark, and full analytical procedures are reported in Bizzarro *et al.* [17]. Samples were aspirated into the plasma source by means of an Apex sample introduction system with an uptake rate of ∼50 µL/min, and the Mg isotope composition was measured in high-resolution mode (M/ΔM > 5000). Using this approach, the sensitivity of the instrument was ∼200 V ppm^{-1} and samples were typically analyzed with a signal intensity ranging from 35 to 100 V on mass ^{24}Mg. Single analyses comprised 1667s of data acquisition followed by 570s of baseline measurements obtained on-peak. Each sample was bracketed by standard analyses and systematically analyzed ten times. Mg isotope data are reported in the µ-notation as relative deviations from the DTS-2b standard ($\mu^{25}\mathrm{Mg}_{DSM-3}$ = −122±17 ppm, 2SD, [17])

according to the following formula:

$$\mu^{x}\mathrm{Mg} = \left[\frac{(^{x}\mathrm{Mg}/^{24}\mathrm{Mg})_{\mathrm{sample}}}{(^{25}\mathrm{Mg}/^{24}\mathrm{Mg})_{\mathrm{DTS\text{-}2}}} - 1\right] \times 10^{6}$$

Where x represent mass 25 or 26. The mass-independent component in ^{26}Mg (μ^{26}Mg*) is reported in the same fashion, but represents deviations from the internally normalized ^{26}Mg/^{24}Mg of the sample from the reference standard, normalized to ^{25}Mg/^{24}Mg = 0.126896 [17] using the exponential mass fractionation law. All Mg data reduction was conducted off-line using the freely distributed Iolite data reduction package which runs within Igor Pro [19] and changes in mass bias with time were interpolated using a smoothed cubic spline. For each analysis, the mean and standard error of the measured ratios were calculated using a 3 SD threshold to reject outliers. Individual analyses of a sample were combined to produce an average weighted by the propagated uncertainties of individual analyses and reported final uncertainties are the 2SE of the mean. The external reproducibility of our measurements using this method is 20 and 2.5 ppm for the μ^{25}Mg and μ^{26}Mg*, respectively [17]. The ^{27}Al/^{24}Mg ratios were measured on an X-series ICP-MS at the Centre for Star and Planet Formation and are accurate to 2%.

The isotopic composition of the purified Cr was determined using the Triton TIMS at the Centre for Star and Planet Formation, Natural History Museum of Denmark, using a sample standard bracketing approach. Cr was dissolved and heat-pretreated for >1 hours in ∼10 M HCl prior to mixing into a silica gel-boric acid-aluminium slurry that was subsequently loaded onto single W-filaments (pre-outgassed for 2 hours at 4.5 A). Prior to loading, the filaments were heated with a ∼2.5 A current and dabbed with parafilm plastic in order to prevent the sample slurry from spreading on the filament. Samples were then loaded at a current of ∼2 A to provide rapid dry-down without actual boiling. After loading and dry-down, the filaments were briefly heated to > 4 A in order to burn of the parafilm brackets and oxidize residual organics from the sample chemistry.

During analysis, the filaments were automatically heated, focused and trimmed to ∼250 mV ^{52}Cr before rapid ramping to ∼10 V ^{52}Cr using the total evaporation mode control. This voltage was maintained until the mass spectrometer software could no longer support it with a current ramp of ∼8 mA/sec. During analysis, ^{50}Cr, ^{52}Cr, ^{53}Cr, ^{54}Cr, ^{51}V and ^{56}Fe were collected on Faraday cups linked to 10^{11} Ohm resistors, while ^{49}Ti was collected on a Faraday cup linked to a 10^{12} Ohm resistor. Data reduction was carried out offline utilizing the Iolite data reduction package, and included correction for ^{50}Ti, ^{50}V and ^{54}Fe. We only included the emission where ^{52}Cr was stable at ∼10 V. We never observed any significant ^{49}Ti or ^{51}V, while ^{56}Fe was typically <10 mV. Each sample measurement consists of the average and standard error of at least 10 individual ∼20 ng filament loads, calculated using a 2 SD outlier rejection scheme. Sample analyses were interspaced with analyses of ∼0 ng filament loads of the SRM-3112a standard, measured under the same conditions as the samples. Individual analyses typically consist of 500s to 1500s of data acquisitions, with typical internal precision of 20 ppm for the ^{54}Cr/^{52}Cr ratio. Electronic baselines were measured at the beginning and end of individual sessions. The ^{54}Cr/^{52}Cr data are reported in the μ notation according to the following formula:

$$\mu^{54}\mathrm{Cr} = \left[\frac{(^{54}\mathrm{Cr}/^{52}\mathrm{Cr})_{\mathrm{sample}}}{(^{54}\mathrm{Cr}/^{52}\mathrm{Cr})_{\mathrm{SRM\text{-}3112a}}} - 1\right] \times 10^{6}$$

Where the ^{54}Cr/^{52}Cr values reflect the internally normalized values, normalized to ^{52}Cr/^{50}Cr = 19.2832 [20] using the exponential mass fractionation law. The uncertainties of the ^{54}Cr/^{52}Cr measurements quoted in Table reflect the internal precision of the measurement. This approach provides several advantages as compared to traditional methods (i.e. [20]). First and foremost, total evaporation mode ensures rapid and reproducible measurement of >90% of the transmitted sample, which is critically important for measurements of small samples such as clasts and small chondrules. The total evaporation mode also stabilizes the sample current within a very narrow intensity window, which alleviates the need for frequent baseline measurements; variations in baselines and other machine parameters are instead corrected by the standard bracketing approach. Finally, the dilution across multiple filaments allows repeat measurements and minimizes the impact of filament poisoning by remaining resin-derived organics.

The accuracy and external reproducibility of our measurements was determined by repeated analyses of column-processed Ivuna CI chondrite and terrestrial rock standards (DTS-2b and BHVO-2). To ensure that the experiments were representative, we used quantifies of magnesium and chromium comparable to that present in the smallest samples analyzed in our study, which are represented by the Isheyevo matrix clasts (∼7.5 μg Mg and ∼200 ng Cr). These were processed individually through our Mg and Cr purification procedure and analyzed by MC-ICPMS and TIMS under the same analytical conditions as the unknowns. Results from these experiments are presented in Table S4. The five sample digestions of the Ivuna CI chondrite yield and average μ^{26}Mg* of 4.7 ppm, which is identical to the average μ^{26}Mg* value of 4.5±2.5 ppm previously obtained for the analysis of 3 CI chondrites, including Ivuna [21]. Moreover, the external reproducibility of the five aliquots of Ivuna analyzed here corresponds to 2.9 ppm, which is comparable to that of 2.5 ppm inferred for our method based on a more extensive dataset [17]. The analyses of two aliquots of the DTS-2b rock standard yield μ^{26}Mg* values consistent with the terrestrial composition. Five column-processed aliquots of the DTS-2b yielded μ^{54}Cr consistent with the terrestrial composition. Moreover, the external reproducibility of these five aliquots corresponds to 12 ppm, which we adopt for the μ^{54}Cr measurements reported in our study. Finally, one analysis of the Ivuna CI chondrite yields an μ^{54}Cr value identical to literature data [22]. Thus, we conclude that the Mg and Cr isotope measurements presented in our study are accurate to their stated uncertainties.

1. Krot AN et al. (2002) The CR chondrite clan: implications for early solar system processes. *Meteorit Planet Sci* **37**: 1451–1490.

2. Weisberg MK et al. (1995) The CR chondrite clan. *Proc NIPR Symp Antarct Meteorites* **8**: 11-32.

3. Makide K et al. (2009) Oxygen- and magnesium-isotope compositions of calcium-aluminum-rich inclusions from CR2 carbonaceous chondrites. *Geochim Cosmochim Acta* **73**: 5018–5050.

4. Nagashima K, Krot AN, Huss GR (2014) ^{26}Al in chondrules from CR2 chondrites. *Geochem J* **48**: 561–570.

5. Abreu NM, Brearley AJ (2010) Early solar system processes recorded in the matrices of two highly pristine CR3 carbonaceous chondrites, MET 00426 and QUE 99177. *Geochim Cosmochim Acta* **74**: 1146–1171.

6. Briani G et al. (2013) Short duration thermal metamorphism in CR chondrites. *Geochim Cosmochim Acta* **122**: 267–279.

7. Greshake A et al. (2002) Heavily hydrated lithic clasts in CH chondrites and the related, metal-rich chondrites Queen Alexandra Range 94411 and Hammadah al Hamra 237. *Meteorit Planet Sci* **37**: 281–293.

8. Krot AN, Nagashima K, Petaev MI (2012) Isotopically uniform, O-depleted calcium, aluminum-rich inclusions in CH and CB carbonaceous chondrites. *Geochim Cosmochim Acta* **83**: 159–178.

9. Krot AN et al. (2005) Young chondrules in CB chondrites from a giant impact in the early Solar System. *Nature* **436**: 989–992.

10. Ivanova M et al. (2008) The Isheyevo meteorite: Mineralogy, petrology, bulk chemistry, oxygen, nitrogen, carbon isotopic compositions, and ^{40}Ar-^{39}Ar ages. *Meteorit Planet Sci* **43**: 915–940.

11. Bonal L et al. (2010) Chondritic lithic clasts in the CB/CH-like meteorite Isheyevo: Fragments of previously unsampled parent bodies. *Geochim Cosmochim Acta* **74**: 2500–2522.

12. Briani G, et al. (2009) Pristine extraterrestrial material with unprecedented nitrogen isotopic variation. *Proc Natl Acad Sci USA* **106** (26): 10522–10527.

13. Bonal L, et al. (2010) Highly ^{15}N-enriched chondritic clasts in the CB/CH-like meteorite Isheyevo. *Geochim Cosmochim Acta* **74**: 6590–6609.

14. Krot AN et al. (2010) Oxygen isotopic compositions of chondrules from the metal-rich chondrites Isheyevo (CH/CBb), MAC 02675 (CBb) and QUE 94627 (CBb). *Geochim Cosmochim Acta* **74**: 2190–2211.

15. Sugiura N et al. (2010) Mn/Cr relative sensitivity factors for synthetic calcium carbonate measured with a NanoSIMS ion microprobe. *Geochem J* **44**: e11–e16.

16. Ogliore RC, Huss GR, Nagashima K (2011) Ratio estimation in SIMS analysis. *Nucl Instrum Meth B* **269**: 1910–1918.

17. Bizzarro M, et al. (2011) High-precision Mg-isotope measurements of terrestrial and extraterrestrial material by HR-MC-ICPMS implications for the relative and absolute Mg-isotope composition of the bulk silicate earth. *J Anal At Spectrom* **26**:565–577.

18. M. Schiller et al. (2014) Precise measurement of chromium isotopes by MC-ICPMS. *J Anal At Spectrom* **29**: 1406–1416.

19. Paton C et al. (2011) Iolite: Freeware for the visualisation and processing of mass spectrometric data. *J Anal At Spectrom* **26**: 2508–2518.

20. Trinquier A, Birck J-L, Allgre CJ (2008) High-precision analysis of chromium isotopes in terrestrial and meteorite samples by thermal ionization mass spectrometry. *J Anal At Spectrom* **23**:1565–1574.

21. Larsen, KK et al. (2011) Evidence for magnesium isotope heterogeneity in the solar protoplanetary disk. *Astrophy J* **735**: L37–L44.

22. Trinquier A, Birck J-L, Allgre C (2007) Widespread ^{54}Cr heterogeneity in the inner solar system. *Astrophys J* **655**: 1179–1185.

23. Zolensky M, Barrett R, Browning L (1993) Mineralogy and composition of matrix and chondrule rims in carbonaceous chondrites. *Geochim Cosmochim Acta* **57**: 3123–3148.

24. Weisberg MK et al. (1993) The CR (Renazzo-type) carbonaceous chondrite group and its implications. *Geochim Cosmochim Acta* **57**: 1567–1586.

25. Bunch TE, Chang S (1980) Carbonaceous chondrites-II. Carbonaceous chondrite phyllosilicates and light element geochemistry as indicators of parent body processes and surface conditions. *Geochim Cosmochim Acta* **44**: 1543–1577.

26. Fujiya W et al. (2013) Evidence for the late formation of hydrous asteroids from young meteoritic carbonates. *Nature Comm* **3**: 627.

27. Fujiya W et al. (2013) Mn-Cr ages of dolomites in CI chondrites and the Tagish Lake ungrouped Carbonaceous chondrite. *Earth Planet Sc Lett* **362**: 130–142.

28. Jilly CE et al. (2013) In Situ Radiometric Dating of Aqueously Formed Carbonates in Sutter's Mill. *Meteorit Planet Sci Supp, Abstract* **76**: 5303.

29. McKibbin SJ, Ireland TR, Amelin Y, Holden P, Sugiura N (2013) A re-evaluation of the MnCr systematics of olivine from the angrite meteorite DOrbigny using Secondary Ion Mass Spectrometry. *Geochim Cosmochim Acta* **123**: 181–194.

30. Steele RCJ, McKeegan, KD (2014) Aqueous alteration on the the CI parent body: Mn-Cr ages of secondary carbonate formation. *77th Annual Meteoritical Society Meeting* Abstract 5438.

31. Ichimura K, Sugiura N (2015) Preparation of synthetic dolomite for determination of Mn/Cr relative sensitivity. 46th *Lunar and Planetary Science Conference*, Abstract 1795.

Table S1. Representative average compositions of (fine-grained) phyllosilicate matrices of nine hydrated lithic clasts (in wt%). N=number of individual analyses.

Clast	N	SiO_2	TiO_2	Al_2O_3	FeO	MnO	MgO	CaO	Na_2O	SO_3	Cr_2O_3	Total
A5003	9	34.19	0.03	2.45	24.72	0.07	18.22	0.09	0.06	1.80	0.54	82.16
A5002	8	34.35	0.02	2.21	21.90	0.06	22.92	0.12	0.06	0.54	0.50	82.69
A5001	6	35.63	0.03	1.49	21.96	0.15	23.49	0.11	0.06	0.46	0.26	83.64
A5004	4	23.34	0.01	1.44	37.76	0.01	15.07	0.13	0.17	3.36	0.23	81.53
A5C001	5	34.63	0.05	1.82	23.03	0.02	22.47	0.10	0.08	0.50	0.27	82.97
B5004	5	35.55	0.03	2.30	19.01	0.04	24.99	0.12	0.04	0.41	0.37	82.85
A3002	10	33.66	0.01	2.80	20.47	0.21	23.52	0.14	0.08	0.58	0.38	81.85
A1001	4	32.59	0.04	1.90	20.57	0.37	22.01	2.03	0.60	4.76	0.35	85.22
A4001	7	32.74	0.02	2.71	24.88	0.04	20.92	0.16	0.05	2.00	0.31	83.83

Table S2. Average chemical compositions (in wt%) of carbonates present in Isheyevo lithic clasts used for Mn-Cr systematics. N is the number of analyses on each carbonate.

Clast	Carbonate	N	CaO	MgO	FeO	MnO	SiO_2	CO_2	Total
A3002	carb-1	12	33.26	13.82	3.57	4.89	0.02	45.22	100.79
	carb-2	13	33.21	13.07	3.61	6.55	0.05	44.80	101.29
B1003	carb-1	3	27.12	16.40	4.85	3.99	0.05	46.32	98.73
I4LC2	carb-1	1	27.19	19.25	2.27	3.96	0.00	46.80	99.47
	carb-2	1	27.02	19.49	2.58	4.10	0.08	46.67	99.93
I4LC3	carb-1	1	29.01	19.25	2.80	2.71	0.00	46.57	100.33

Table S3. Manganese and chromium isotope data from six dolomites in four hydrated lithic clasts in Isheyevo. Chromium isotope compositions are given in the δ-notation, which reflects the permil deviation (‰) from the terrestrial standard. Columns for ^{55}Mn, ^{52}Cr and ^{53}Cr represent total counts. Errors on $^{55}Mn/^{52}Cr$ and δ^{53}Cr are given in 2σ represent the external reproducibility or the internal precision, whichever is larger. Quoted $^{55}Mn/^{52}Cr$ errors include uncertainties associated with the RSF. N is the spot number on the carbonate grains.

Carbonate	N	^{55}Mn	^{52}Cr	^{53}Cr	$^{55}Mn/^{52}Cr$	δ^{53}Cr (‰)
A3002-1	1	4.11E+06	1824	218	3190±638	61±24
	2	4.93E+06	239	46	29370±5874	698±95
	3	6.84E+06	1653	210	5885±1177	132±23
	4	1.71E+06	1352	158	1803±361	46±28
A3001-2	1	9.43E+06	1920	246	6992±1398	145±24
B1d003-1	1	3.57E+06	92865	10431	60±12	15±5
B1d003-2	1	3.50E+06	62644	7039	87±17	16±6
I4LC2	1	3.38E+06	3597	410	1450±290	31±19
	2	3.20E+06	23575	2639	211±42	12±8
I4LC3	1	1.52E+06	793	95	3006±601	86±32

Table S4. Magnesium and chromium isotope composition of terrestrial standards and the Ivuna CI chondrite. N, number of individual analyses.

Sample	Type	$^{27}Al/^{24}Mg$	μ^{26}Mg*	μ^{25}Mg	N	μ^{54}Cr	N
DTS-2b (1)	Dunite		-1.9±1.4	-27±4	10	-2±5	7
DTS-2b (2)	Dunite		0.5±2.4	4±18	10	-6±13	10
DTS-2b (3)	Dunite					0±17	9
DTS-2b (4)	Dunite					4±11	10
DTS-2b (5)	Dunite					9±14	10
BHVO-2 (1)	Basalt					-2±28	8
BHVO-2 (2)	Basalt					6±13	9
Ivuna (1)	CI	0.093	2.6±5.2	-70±4	8	159±14	12
Ivuna (2)	CI		4.9±2.9	-33±9	10		
Ivuna (3)	CI		5.3±3.2	-122±7	10		
Ivuna (4)	CI		4.3±3.9	-131±3	10		
Ivuna (5)	CI		6.6±3.3	-82±6	10		

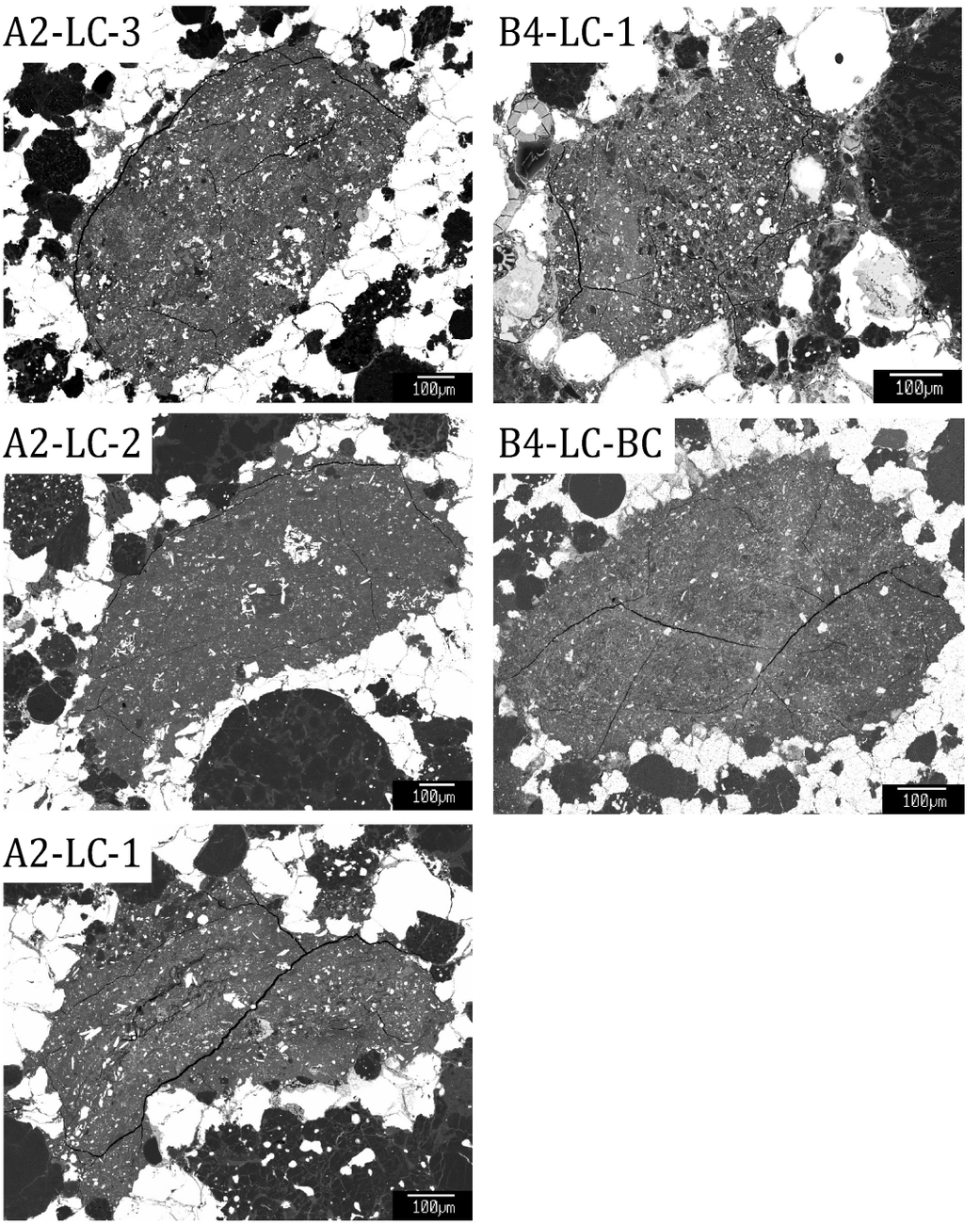

Fig. S1. Back-scattered electron (BSE) images of five hydrated lithic clasts from the Isheyevo CH/CB chondrite sampled for Mg- and Cr-isotope analyses.

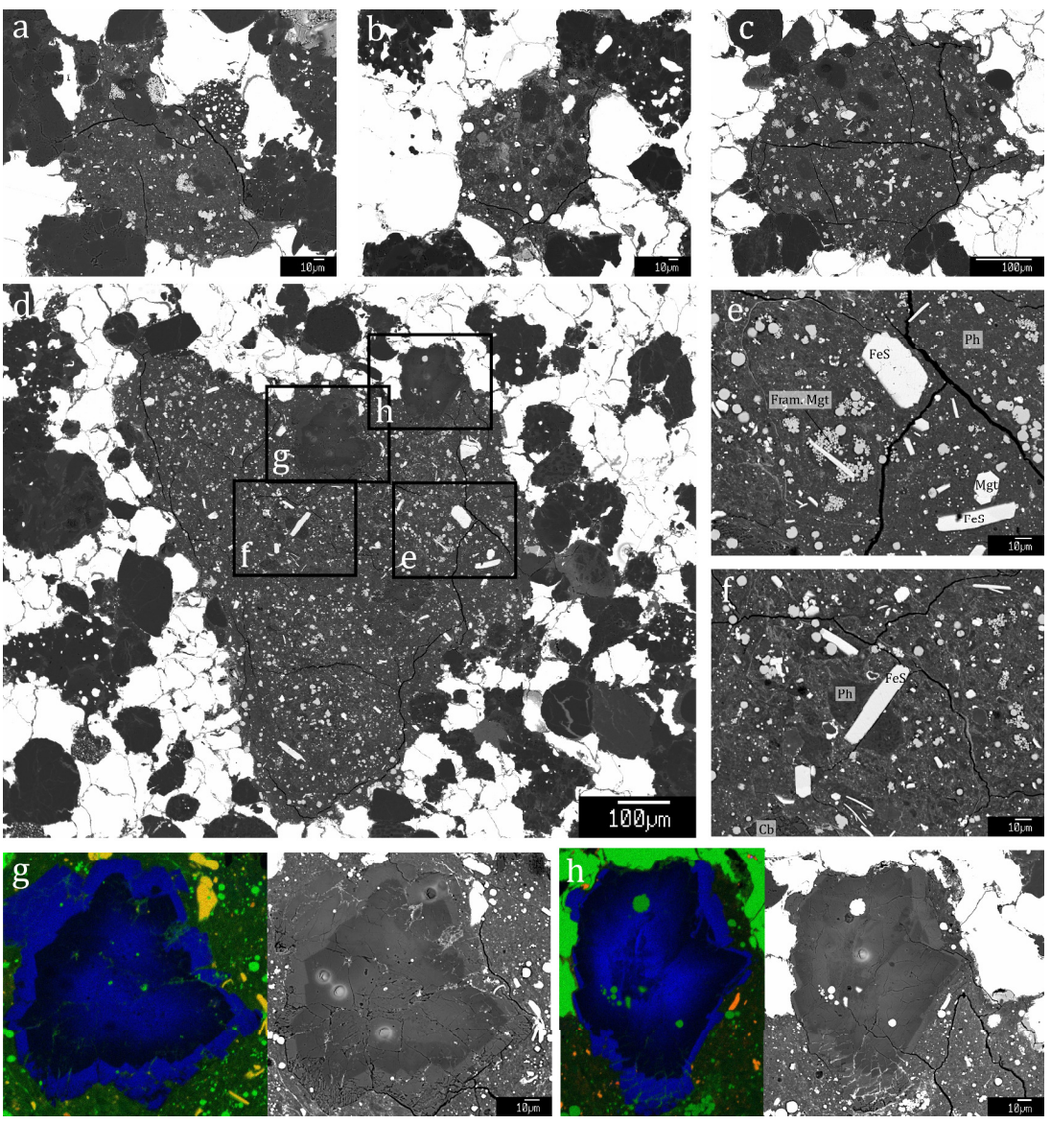

Fig. S2. SBSE images of four hydrated lithic clasts (a-d) and their components (e-h), selected for in situ Mn-Cr measurements on carbonates. A zoom in on one lithic clast (d) shows the presence of platy sulfides (FeS), framboidal magnetite (Fram. Mgt), magnetite (Mgt) and dolomitic carbonates (Cb) in a phyllosilicate matrix (Ph) (e-f). Carbonates (g-h) are shown as Mn-Fe-S (blue-green-red) x-ray elemental maps and as BSE images with ion probe pits.

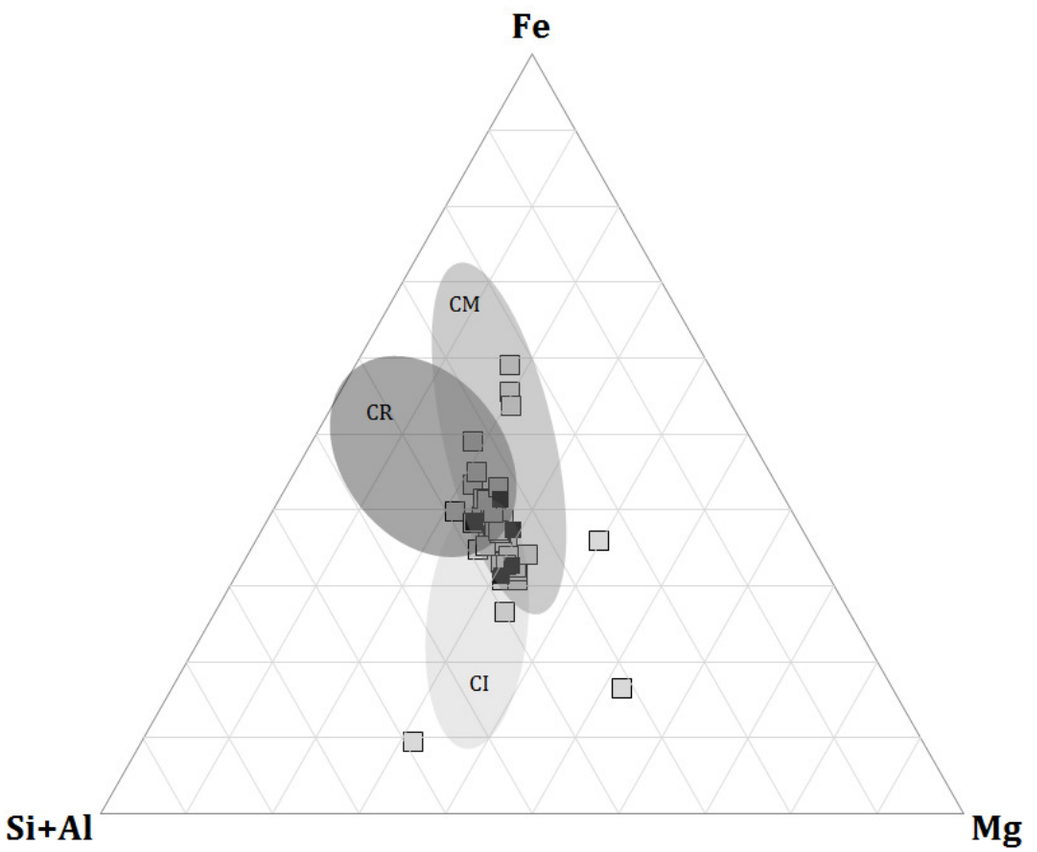

Fig. S3. Phyllosilicate compositions of lithic clasts in ternary diagram with end-member compositions of relative abundances of Fe, Mg and Si+Al, calculated from their weight percentages. Black squares represent hydrated lithic clasts after [11] and grey squares are lithic clast compositions from this work. The compositional fields of CR, CM and CI chondrites are also plotted, including data from [23,24,25].

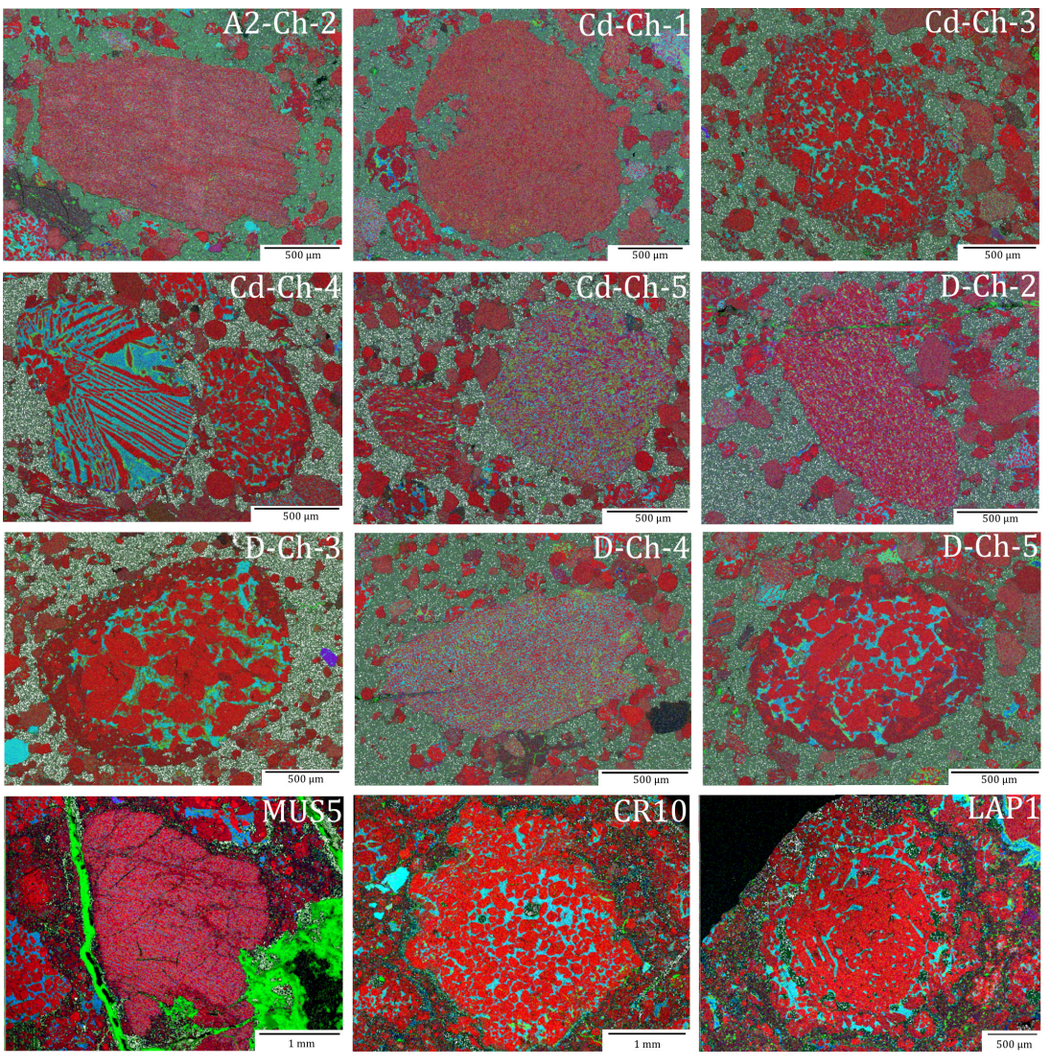

Fig. S4. Combined Mg Al Ca (red-blue-green) x-ray elemental images of nine Isheyevo chondrules (A2-Ch-1, Cd-Ch-2, Cd-Ch-5, D-Ch-2 and D-Ch-4 are skeletal, Cd-Ch-4 is barred and Cd-Ch-3, D-Ch-3 and D-Ch-5 are porphyritic) and three chondrules from CR chondrites (CR10 and LAP1 are porphyritic and MUS5 is skeletal) sampled for Mg- and Cr-isotope analyses. The color scheme for chondrule MUS5 is slightly unbalanced due to a Ca-rich vein crossing the image.

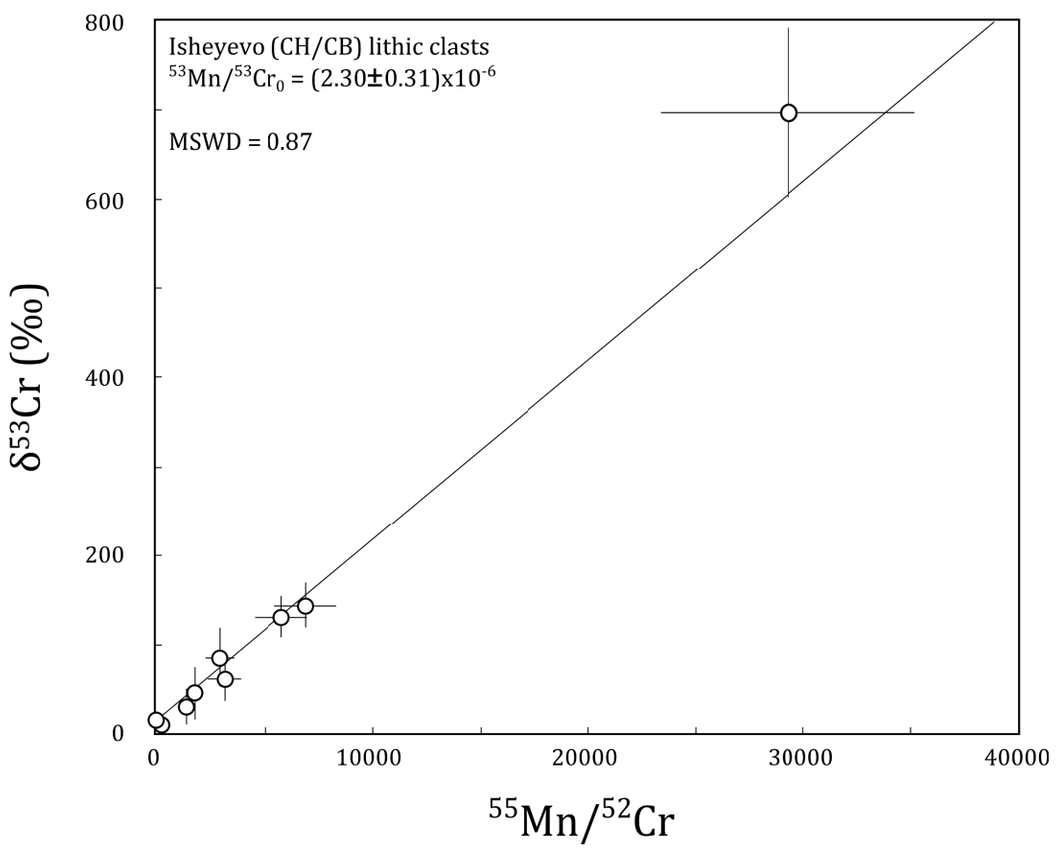

Fig. S5. $^{55}Mn/^{52}Cr$ versus $\delta^{53}Cr$ diagram plotted for 10 analyses on 6 dolomites from 4 lithic clasts. Errors are 2σ.

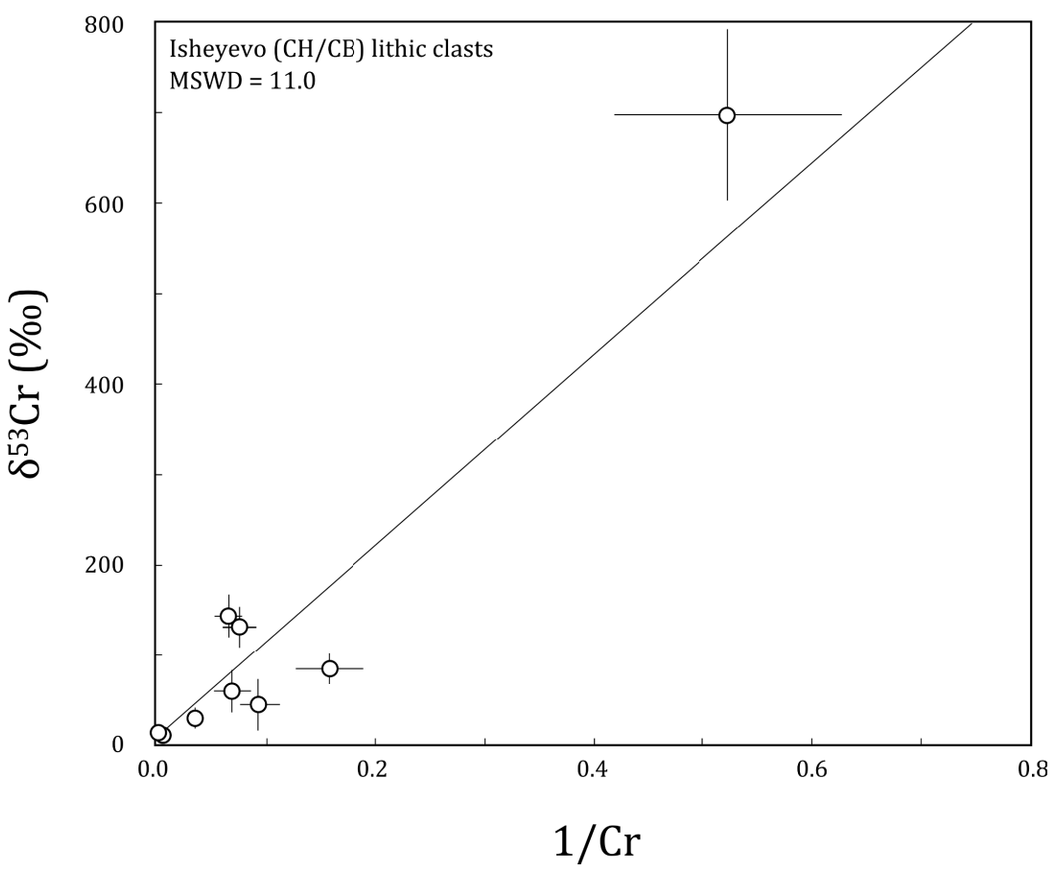

Fig. S6. 1/Cr versus δ^{53}Cr diagram plotted for 10 analyses on 6 dolomites from 4 lithic clasts. Errors are 2σ. The MSWD value (11.0) is significantly larger than for Figure S5, suggesting that the correlation between $^{55}Mn/^{52}Cr$ and δ^{53}Cr defines an isochron.

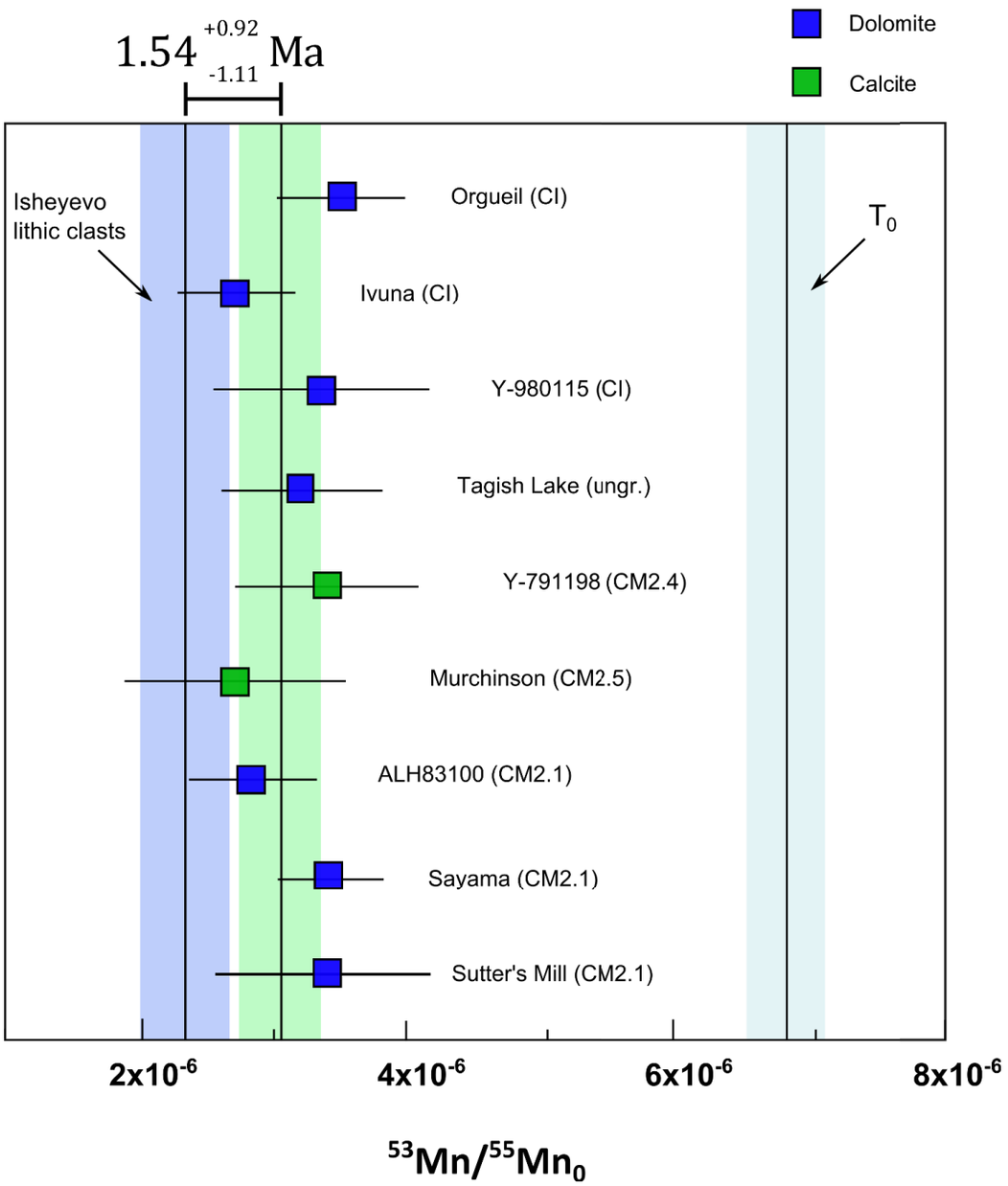

Fig. S7. $^{53}Mn/^{55}Mn$ initial ratios for dolomites and calcites in CI and CM chondrites [26,27,28] and Isheyevo lithic clasts (blue bar, this work). The weighted average for $^{53}Mn/^{55}Mn_0$ from CI and CM chondrites is represented by a green bar and the $^{53}Mn/^{55}Mn_0$ for T_0 is inferred from CV CAIs relative to the D'Orbigny angrite [29], as represented by a grey bar. However, we note that it has recently been suggested that the relative sensitivity factor of the Mn/Cr for dolomite may be different from that of calcite [30,31]. Thus, the age we report and its uncertainty may be subject to adjustment.

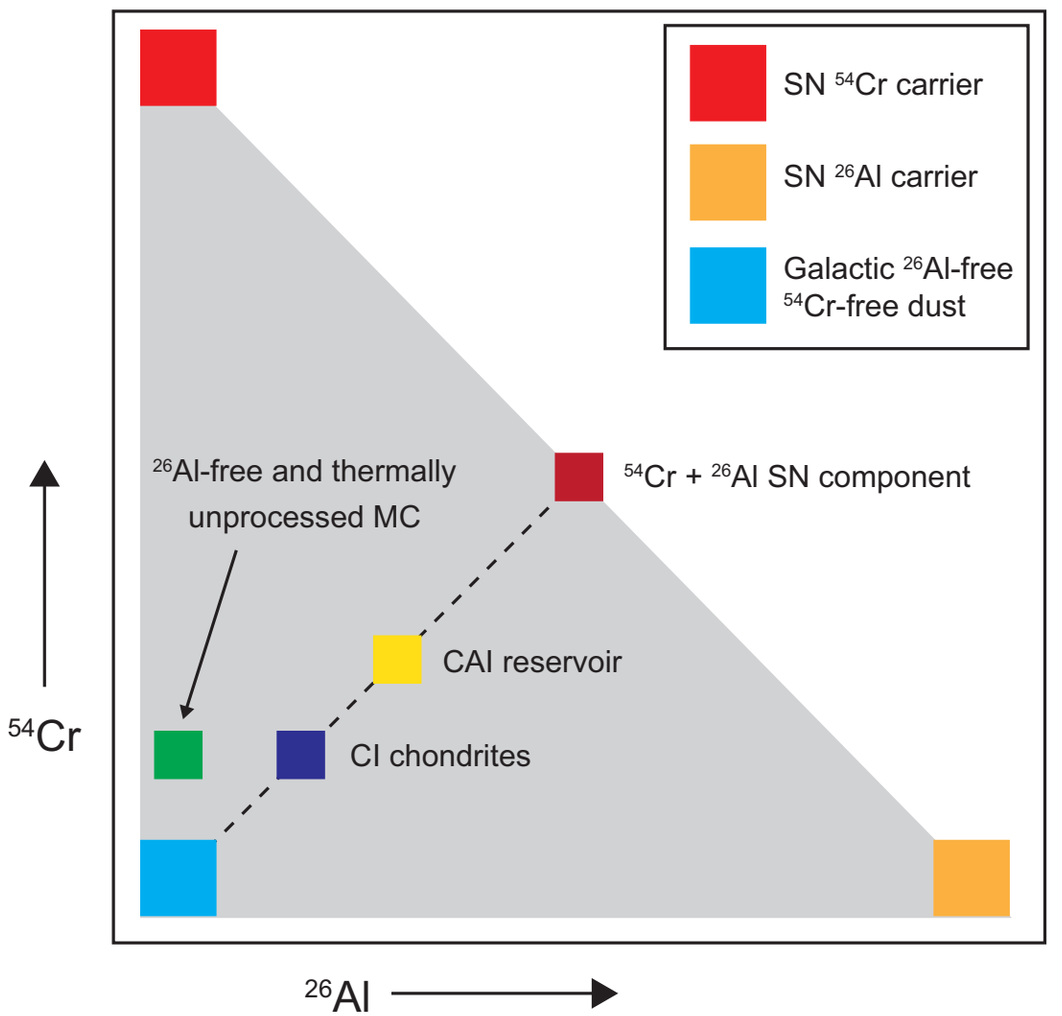

Fig. S8. Cartoon illustrating the different end member compositions as possible and observed mixtures of these components. Three components are required to explain the range of compositions, namely distinct presolar ^{54}Cr and ^{26}Al carriers and a galactic background component. We infer that the ^{54}Cr and ^{26}Al carriers represent young supernova (SN) dust generation produced during the lifetime of the giant molecular cloud. The galactic background component reflect older dust lacking the new SN component. The thermal processing, which is represented by the dashed line, reflects the binary unmixing of a new dust comment mixture contain both the individual ^{26}Al and ^{54}Cr carriers and the galactic background component. Our model assumes that the binary unmixing of the two dust components results in linear array, which requires that the ^{26}Al and ^{54}Cr carriers have similar thermal properties. This is assumption is consistent with the data presented in Fig.1 of the main paper. However, the unmixing relationship may not result in a linear array if, for example, the ^{26}Al carrier is more refractory than the ^{54}Cr carrier.